Noncovalent Mechanism for the Conformal Metallization of Nanostructured Parylene Films

ARTICLE *in* LANGMUIR · MARCH 2010

Impact Factor: 4.46 · DOI: 10.1021/la9034529 · Source: PubMed

Langmuir
Article
pubs.acs.org/Langmuir

Noncovalent Mechanism for the Conformal Metallization of Nanostructured Parylene Films

Niranjan A. Malvadkar,[†] Koray Sekeroglu,[†] Walter J. Dressick,[‡] and Melik C. Demirel*,[†]

[†]*Materials Research Institute and Department of Engineering Science and Mechanics, Pennsylvania State University, University Park, Pennsylvania 16802, and* [‡]*Naval Research Laboratory, Code 6910, 4555 Overlook Avenue, S.W., Washington, D.C. 20375*

Received September 13, 2009. Revised Manuscript Received December 17, 2009

We describe a rapid, reliable method of preparing nanoporous Ni or Co films using nanostructured poly(chloro-*p*-xylylene) (nanoPPX) films as templates. The nanoPPX films are vapor deposited onto Si substrates using oblique angle polymerization (OAP), resulting in the formation of an obliquely aligned PPX nanorod array on the substrate. The nanoPPX films are then subjected to noncovalent functionalization using an aromatic ligand (i.e., pyridine) by means of treatment with either an aqueous solution of the ligand or ligand vapor. The results of quartz crystal microbalance and X-ray diffraction studies support a model in which pyridine adsorption is facilitated by the formation of $\pi-\pi$ interactions with aromatic moieties in the amorphous surface regions of nanoPPX. The physisorbed pyridine in the nanoPPX film can subsequently bind a catalytic Pd(II)-based colloidal seed layer. Continuous, conformal Ni or Co films, characterized by FIB/SEM and AFM, are grown on the Pd(II)-laden nanoPPX films using electroless metallization. Analogous metallization of a conventionally deposited planar PPX film results in noncontinuous or patchy metal deposits. Such behavior is attributed to the sluggish adsorption of pyridine in the planar PPX film, resulting in an ~22-fold decrease in the quantity of pyridine adsorbed compared to that in a nanoPPX film. Consequently, the level of Pd(II) bound by pyridine on a planar PPX film is insufficient to catalyze continuous metallization. Results of a statistical two-level factorial design indicate that the morphology of the metal layer formed on a nanoPPX film is profoundly influenced by the ligand adsorption condition (i.e., aqueous ligand vs ligand vapor treatment) and is correlated to the catalytic activity of Co films for the production of hydrogen from sodium borohydride decomposition.

1. Introduction

Electroless metallization is a technique used to deposit metal layers on the surfaces of polymers using an autocatalytic reduction reaction of metal ions without the application of an external electric source.[1−5] The process is simple, does not require sophisticated equipment, and can be carried out under ambient conditions. In general, the electroless metallization reaction occurs on catalytic sites present on the substrate, as described further below. The overall metallization reaction can be written as

$$M^{n+} + ne^{-}(\text{from reducing agent}) \rightarrow M^{0} \qquad (1)$$

Metallized polymer surfaces prepared by electroless metallization have applications in a wide variety of areas, including microfabrication,[6−10] biomedical devices,[11,12] catalysis,[13] automotive,[14] and food packaging.[15] The metal/polymer interface properties are therefore an important consideration during the manufacturing of such components. Obtaining a good metal/polymer interface is often a challenge because of the chemical incompatibilities between many metals and polymers.[9,16−18] Poor adhesion of metal layers to polymer surfaces limits the use of electroless metallization for many practical applications. Attaining acceptable metal/polymer interface adhesion usually requires prior chemical pretreatment of the polymer surfaces through techniques such as excimer UV,[19−21] laser ablation,[22] plasma,[23−25] wet chemical treatments,[26] and/or microscopic roughening to

*Corresponding author. Tel: (814) 863-2270. Fax: (814) 865-9974. E-mail: mdemirel@engr.psu.edu.

(1) Lowenhaim, F. A. *Modern Electroplating*; John Wiley & Sons: New York, 1974.
(2) Mallory, G. O., Hajdu, J. B., Eds. *Electroless Plating: Fundamentals and Applications*; American Electroplaters and Surface Finisher's Society: Orlando, FL, 1990.
(3) Gavrilov, G. G. *Chemical* (*Electroless*) *Nickel-Plating*; Portcullis Press: London, 1979.
(4) Duffy, J. I. *Electroless and Other Nonelectrolytic Plating Techniques: Recent Developments*; Noyes Data Corp: Park Ridge, NJ, 1980.
(5) Zabetakis, D.; Dressick, W. J. *ACS Appl. Mater. Interfaces* **2009**, *1*, 4–25.
(6) Cheng, K.; Yang, M. H.; Chiu, W. W. W.; Huang, C. Y.; Chang, J.; Ying, T. F.; Yang, Y. *Macromol. Rapid Commun.* **2005**, *26*, 247–264.
(7) Wu, S. Y.; Kang, E. T.; Neoh, K. G.; Tan, K. L. *Langmuir* **2000**, *16*, 5192–5198.
(8) Shafeev, G. A.; Themlin, J. M.; Bellard, L.; Marine, W.; Cros, A. *J. Vac. Sci. Technol., A* **1996**, *14*, 319–326.
(9) Sacher, E. *Prog. Surf. Sci.* **1994**, *47*, 273–300.
(10) Shachamdiamand, Y.; Dubin, V.; Angyal, M. *Thin Solid Films* **1995**, *262*, 93–103.
(11) Gray, J. E.; Norton, P. R.; Griffiths, K. *Thin Solid Films* **2005**, *484*, 196–207.
(12) Sipaut, C. S.; Ibrahim, M. N. M.; Izat, M. E. *J. Appl. Polym. Sci.* **2007**, *103*, 1554–1565.
(13) Malvadkar, N.; Park, S.; Urquidi-MacDonald, M.; Wang, H.; Demirel, M. C. *J. Power Sources* **2008**, *182*, 323–328.
(14) McCaskie, J.; Redding, S. *Met. Finish* **2008**, *106*, 25–27.
(15) Zhao, Q.; Wang, C.; Liu, Y.; Wang, S. *Int. J. Adhes. Adhes.* **2007**, *27*, 85–91.
(16) Mittal, K. L. *J. Vac. Sci. Technol.* **1976**, *13*, 19–25.
(17) Wu, S. Y.; Kang, E. T.; Neoh, K. G.; Han, H. S.; Tan, K. L. *Macromolecules* **1999**, *32*, 186–193.
(18) Bou, M.; Martin, J. M.; Lemogne, T. *Appl. Surf. Sci.* **1991**, *47*, 149–161.
(19) Charbonnier, M.; Romand, M.; Esrom, H.; Seebock, R. *J. Adhes.* **2001**, *75*, 381–404.
(20) Beil, S.; Horn, H.; Windisch, A.; Hilgers, C.; Pochner, K. *Surf. Coat. Technol.* **1999**, *116*, 1195–1203.
(21) Weichenhain, R.; Wesner, D. A.; Pfleging, W.; Horn, H.; Kreutz, E. W. *Appl. Surf. Sci.* **1997**, *110*, 264–269.
(22) Niino, H.; Yabe, A. *Appl. Surf. Sci.* **1993**, *69*, 1–6.
(23) Charbonnier, M.; Romand, M.; Harry, E.; Alami, M. *J. Appl. Electrochem.* **2001**, *31*, 57–63.
(24) Inagaki, N.; Tasaka, S.; Park, Y. W. *J. Adhes. Sci. Technol.* **1998**, *12*, 1105–1119.
(25) Zettsu, N.; Itoh, H.; Yamamura, K. *Surf. Coat. Technol.* **2008**, *202*, 5284–5288.
(26) Kang, E. T.; Zhang, Y. *Adv. Mater.* **2000**, *12*, 1481–1494.

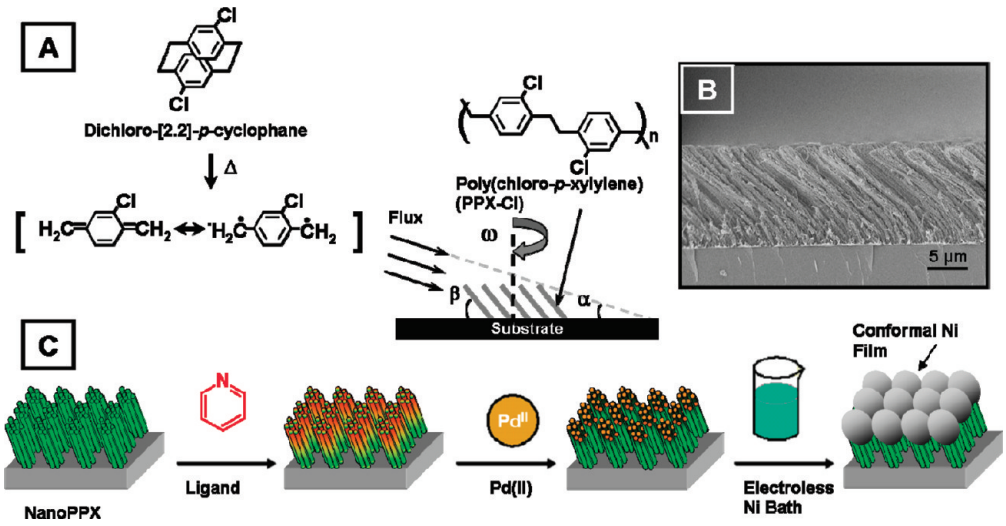

Figure 1. (A) Schematic depicting the formation of a poly(chloro-*p*-xylylene) (PPX) film template using dichloro-*p*-cyclophane as the precursor. Oblique angle polymerization (OAP) is used to grow the nanoPPX films on a silicon substrate. (B) Cross-sectional SEM image of nanoPPX film showing the parallel nanorod growth on the silicon substrate. (C) Schematic of the formation of a Ni film on nanoPPX via the noncovalent electroless metallization process.

promote metal anchoring to the film.[2] The roughening is usually carried out by techniques such as mechanical roughening,[27] laser treatment,[28] low-energy ion treatment,[29] chemical etching,[30−32] phase-separation-induced roughening,[33] silver nanopowder coating,[34] and photolithography.[35]

These roughened polymer films are then chemically functionalized by the adhesion of functional species that catalyze the electroless metallization process. Typically, the functional species consists of a commercial bimetallic colloid with a low-valent Pd core and a Sn-ion-rich polymeric shell.[36,37] Although the low-valent Pd core promotes the initiation of the metallization process, the Sn ion surface binds the colloid to the roughened polymer surface.[38] To initiate the metallization reaction, the Pd core must first be exposed after the adsorption of the bimetallic colloid on the polymer surface. This requires an extremely controlled reaction in which an "acceleration" agent such as fluoroboric acid is used to dissolve a sufficient amount of the Sn shell to expose the Pd core without removing that portion of the Sn anchoring the catalyst to the substrate. Finally, metallization is carried out using commercially available electroless baths consisting of a source of metal ions, a reducing agent, a complexing agent, and a stabilizer or inhibitor.[2] Although the entire electroless metallization processes on an industrial scale is highly optimized, it is always advantageous to reduce the number of processing steps without compromising the quality of the metal layer and the interface strength.

We recently demonstrated a quicker method to electrolessly deposit a Ni layer on nanostructured poly(chloro-*p*-xylylene) (nanoPPX) surfaces.[39] The nanoPPX films are grown by a novel vapor-deposition technique called oblique angle polymerization (OAP) (Figure 1A).[40,41] In OAP, the monomeric radical flux generated during the vapor-phase pyrolysis of a dichloro[2.2]-*p*-cyclophane precursor is directed at an angle to the substrate, typically $< 10°$. Polymerization is initiated on the surface of the substrate, and a combination of nucleation, polymerization, geometrical self-shadowing, and surface diffusion influences the growth of the polymer film. The final nanostructure consists of obliquely aligned PPX nanorods on the substrate (Figure 1B).

We used a noncovalent functionalization strategy to deposit a metal layer on the surface of a nanoPPX film (Figure 1C).[39] Our strategy takes advantage of the nanoPPX nanostructured morphology to adsorb ligand molecules into the nanoPPX films via noncovalent attractive forces.[39,42] Afterwards, Pd(II)-based colloids (designated PD1) are allowed to covalently bind to these ligand sites, resulting in the formation of a catalytic seed layer where metal ion reduction takes place. Finally, electroless Ni metallization is carried out using NIPOSIT 468B (a commercial electroless Ni bath).

This approach to electroless metallization is advantageous in several ways. First, the surface morphology possesses a natural roughness created by the aligned nanorods. The rms roughness is a order of magnitude higher than for polymers deposited by conventional vapor-deposition techniques that do not constrain the radical flux.[41] The metal layer deposited onto the nanoPPX film is therefore mechanically anchored by the rough nanoPPX film surface.[39] Second, the component features of nanoPPX exhibit a high curvature that promotes the splaying of adjacent polymer chains, resulting in an amorphous, open surface structure conducive to noncovalent ligand binding. The high surface

(27) Yu, W. X.; Hong, L.; Chen, B. H.; Ko, T. M. *J. Mater. Chem.* **2003**, *13*, 818–824.
(28) Horn, H.; Beil, S.; Wesner, D. A.; Weichenhain, R.; Kreutz, E. W. *Nucl. Instrum. Methods Phys. Res., Sect. B* **1999**, *151*, 279–284.
(29) Zaporojtchenko, V.; Zekonyte, J.; Faupel, F. *Nucl. Instrum. Methods Phys. Res., Sect. B* **2007**, *265*, 139–145.
(30) Siau, S.; Vervaet, A.; Van Calster, A.; Swennen, I.; Schacht, E. *J. Electrochem. Soc.* **2004**, *151*, J54–J61.
(31) Ge, J.; Turunen, M. P. K.; Kivilahti, J. K. *J. Polym. Sci., Part B: Polym. Phys.* **2003**, *41*, 623–636.
(32) Vorobyova, T. N. *J. Adhes. Sci. Technol.* **1997**, *11*, 167–182.
(33) Saraf, R. F.; Roldan, J. M.; Derderian, T. *IBM J. Res. Dev.* **1994**, *38*, 441–456.
(34) Chung, C. K.; Fung, P. K.; Hong, Y. Z.; Ju, M. S.; Lin, C. C. K.; Wu, T. C. *Sens. Actuators, B* **2006**, *117*, 367–375.
(35) Vaeth, K. M.; Jensen, K. F. *Chem. Mater.* **2000**, *12*, 1305–1313.
(36) Cohen, R. L.; West, K. W. *J. Electrochem. Soc.* **1973**, *120*, 502–508.
(37) Holderer, O.; Epicier, T.; Esnouf, C.; Fuchs, G. *J. Phys. Chem. B* **2003**, *107*, 1723–1726.
(38) Cohen, R. L.; West, K. W. *J. Electrochem. Soc.* **1972**, *119*, 433–438.
(39) Demirel, M. C.; Cetinkaya, M.; Singh, A.; Dressick, W. J. *Adv. Mater.* **2007**, *19*, 4495–4499.
(40) Cetinkaya, M.; Malvadkar, N.; Demirel, M. C. *J. Polym. Sci., Part B: Polym. Phys.* **2008**, *46*, 640–648.
(41) Cetinkaya, A.; Boduroglu, S.; Demirel, M. C. *Polymer* **2007**, *48*, 4130–4134.
(42) Chen, M.-S.; Brandow, S. L.; Schull, T. L.; Chrisey, D. B.; Dressick, W. J. *Adv. Funct. Mater.* **2005**, *15*, 1364–1375.

energy associated with the high-curvature nanorods comprising the porous nanoPPX structure allows for the entrapment of ligand molecules (physisorption) in large quantity, thereby increasing the level of the bound Pd(II) seed layer.[39] This results in a large number of nucleation sites for metal reduction, further increasing the interface strength. The excellent polymer/metal interface strength is demonstrated by the Scotch tape adhesion test that shows only 5% metal removal.[39] In contrast, conventionally deposited polymers do not possess the nanostructured roughness that facilitates ligand−molecule binding, thereby showing poor metallization and interface strength. Third, the use of a ligand to bind Pd(II) catalysts eliminates the need for Sn in the catalyst formulation. This provides a more environmentally friendly catalyst system and eliminates the need to perform the difficult HBF_4 acceleration step associated with the use of Pd/Sn catalysts. Last, the metal layer grows conformally on the nanoPPX surface so that the final morphology of the metal layer is largely dictated by that of the underlying polymer, at least for short plating times.

We previously showed that the morphology of the nanoPPX film can be engineered by modifying the monomer chemistry.[40] In addition, changing the deposition parameters such as the substrate tilt and in-plane rotation during nanoPPX film growth results in exotic nanoPPX morphologies such as chevrons and helices.[43] The combination of OAP and noncovalent functionalization offers a method to prepare template-based metal nanostructures at low cost with high tunability of the metal film morphology and simpler processing steps. This method of preparing nanostructured metal surfaces has significant advantages over traditional approaches such as chemical or electrochemical etching techniques that exhibit poor control and tunability over the metal morphology and advanced patterning techniques such as e-beam lithography that are often too complex and expensive for any large-scale application.

In this article, we further test the metal growth model described in our previous communication[39] and refine it on the basis of the current results. Quartz crystal microbalance (QCM), X-ray diffraction (XRD), and adsorption isotherm studies of nanoPPX and planar PPX films are used to probe the ligand-binding mechanism. We verify the nature of the chemical interactions associated with the Pd(II)−ligand binding and subsequent electroless deposition processes via XPS. FIB/SEM and AFM studies, in combination with statistically designed experiments, are then utilized to identify and better understand the factors affecting metal morphology and growth. Last, we show that the ability to control the morphology of the metal layer deposited, primarily via choice of ligand adsorption conditions, can be used in practical applications such as the catalytic decomposition of sodium borohydride for hydrogen production.

2. Experimental Section

2.1. Materials. Deionized water (18.1 MΩ cm) from a Barnstead Nanopure Diamond dispenser was used for all experiments. All materials were ACS reagent grade or equivalent and were used as received. Poly(chloro-*p*-xylylene) (PPX) films were prepared on Si(100) wafers (Wafernet Inc. San Jose, CA) as described below from dichloro-[2,2]paracyclophane (DCPC) purchased from Parylene Distribution Services. NIPOSIT 468B, a proprietary electroless Ni bath, was purchased from Rohm and Haas (Shipley Co.), and a stock solution was prepared according to the manufacturer's instructions immediately prior to use. Co bath components included electroless Co bath components $CoCl_2 \cdot 6H_2O$, NH_4Cl, ethylenediaminetetraacetic acid (EDTA) tetrasodium salt, and the dimethylamine−borane complex (DMAB), and Pd(II) catalyst components $Na_2PdCl_4 \cdot 3H_2O$, 2-(*N*-morpholino)ethanesulfonic acid (MES) buffer, and NaCl were purchased from Alfa Aesar. $NaBH_4$ and NaOH (pellets) required for catalysis experiments were purchased from J. T. Baker Inc. and EMD Chemicals Inc., respectively.

2.2. Substrate Preparation. All work was carried out in a well-ventilated fume hood. Native oxide p-type Si(100) wafers were first sonicated in acetone, rinsed in water, and dried with nitrogen gas to remove any physisorbed contaminants. Later, the wafers were transferred to a 1/1 (v/v) solution of hydrochloric acid and anhydrous methanol. After 30 min, the wafers were removed, rinsed thoroughly in water, dried with nitrogen gas, and kept in sulfuric acid for another 30 min. Wafers were then removed and thoroughly washed with copious amounts of water and dried with nitrogen gas. Wafers were then transferred to an allyltrimethoxysilane self-assembled monolayer (SAM) solution comprising 1% (v/v) allyltrimethoxysilane (Gelest, PA) in toluene containing 0.1% (v/v) acetic acid. The cleaned wafers were left in the SAM solution for 60 min at 25 °C, removed after 60 min, and sonicated in anhydrous toluene for 10 min. The wafers were then dried on a hot plate at 140 °C for 5 min to remove the solvent and complete the chemisorption process. SAM-treated silicon wafers were stored in a dark environment at 5 °C until needed for PPX deposition.

2.3. NanoPPX. NanoPPX films were deposited on the allyl-functionalized silicon substrates using the OAP technique explained in our previous work.[40] Briefly, 0.3 g of DCPC was vaporized at 175 °C, followed by pyrolysis at 690 °C in a tube furnace. The resulting stream of free radicals was directed onto the allyl-functionalized Si wafers held at $\alpha = 10°$ (Figure 1A) in a deposition chamber for polymerization. The entire system (i.e., the vaporization chamber, tube furnace, and deposition chamber) was maintained at low vacuum (~10 Torr) using a rotary pump. Helical nanoPPX films required for the catalyst experiments were prepared by introducing an additional parameter (i.e., axial substrate rotation (rotational speed, $\omega = 5$ rpm; see Figure 1A)) during OAP film growth.[43] Planar PPX films were deposited without angular flux or substrate rotation (i.e., $\alpha = 90°$ and $\omega = 0$ rpm) using 3 g of DCPC while keeping the vaporization and pyrolysis temperature the same as in nanoPPX film preparation.

2.4. Metallization. *2.4.1. Ligand Functionalization.* The functionalization of PPX films was carried out using either aqueous pyridine or vapor pyridine treatment. For aqueous pyridine treatment, the PPX films were soaked in a 1 M aqueous pyridine solution held in a tightly sealed vial for 30 or 48 h. The films were rinsed in water and then transferred to the Pd(II)-based colloidal dispersion for surface catalysis. For vapor-phase pyridine treatment, the PPX samples were suspended in a sealed vial with a few drops of pyridine (not in contact with the samples). The vials were maintained at a temperature of 110 °C (pyridine bp = 115.2 °C) in an oil bath for ~48 h (unless specified otherwise). Unlike aqueous-pyridine-treated PPX films, vapor-pyridine-treated PPX films were directly transferred to the Pd(II)-based colloidal dispersion after being removed from the vials.

2.4.2. Surface Catalysis. PD1, a Pd(II)-based catalyst system, was prepared as described in the literature.[44] Briefly, 11.5 mg of $Na_2PdCl_4 \cdot 3H_2O$ was completely dissolved in 1 mL of 1.00 M NaCl(aq), followed by the addition of 10 mL of pH 5 0.10 M MES buffer. The resulting solution was diluted to 100 mL by the addition of water. This solution was incubated at 25 ± 0.1 °C in a temperature-controlled water bath for 20 h, after which a 10 mL aliquot was removed and replaced with 10 mL of the 1.00 M NaCl(aq) solution. The resultant PD1 catalyst dispersion is stable for up to at least 1 month in the water bath held at 25 ± 0.1 °C. NanoPPX films treated with pyridine were kept in the colloidal dispersion for 45 min (unless specified otherwise), after which they

(43) Demirel, M. C. *Colloids Surf., A* **2008**, *321*, 121–124.

(44) Dressick, W. J.; Kondracki, L. M.; Chen, M. S.; Brandow, S. L.; Matijević, E.; Calvert, J. M. *Colloids Surf., A* **1996**, *108*, 101–111.

were gently rinsed with water for 5−10 s, dried with nitrogen gas, and immediately transferred to the metallization bath.

2.4.3. Electroless Metallization. For Ni metallization, the stock solution of NIPOSIT 468B was diluted to 10% of the original concentration by the addition of water. During Ni deposition, the samples were gently agitated to remove any adhered hydrogen gas bubbles on the surface. Metal deposition was carried out for 5 to 60 min (as specified) at 25 °C, after which the films were rinsed with water, dried with nitrogen gas, and stored in Fluoroware containers until they were used for characterization.

For Co metallization, the pyridine functionalization (aqueous and vapor treatments) was carried out for 48 h and surface catalysis using PD1 was carried out for 45 min on helical nanoPPX films per the procedure described above. After the two treatments, the films were then transferred to the Co bath that had been freshly prepared using a previously reported procedure.[45] Briefly, 0.9 g of EDTA tetrasodium salt, 1 g of NH_4Cl, and 0.6 g of $CoCl_2 \cdot 6H_2O$ were dissolved in 15 mL of water. A dimethylamine-borane (DMAB) solution (0.4 g in 5 mL of water) was then added. The pH of the resultant solution was adjusted to 8.2 by the dropwise addition of a 0.1 M NaOH(aq) solution. Surface-catalyzed helical nanoPPX films were introduced into the solution, and metallization was carried out for the required time at 25 °C. The Co bath was gently agitated during metallization. Co-coated helical nanoPPX films were removed from the bath, rinsed with DI water, dried with N_2 gas, and stored in a vacuum desiccator until required for hydrogen release experiments.

2.5. Characterization. *2.5.1. AFM.* The surface topography was characterized by an atomic force microscope (Nanoscope E, Veeco Inc.) using silicon nitride cantilevers (Veeco Metrology, CA) in contact mode. The rms roughness was recorded for three to six random area scans (5 μm × 5 μm) on each sample. The "Flatten" command in Nanoscope was used before recording the rms roughness to remove any effect due to large-scale surface corrugations on the sample.

2.5.2. FESEM. Cross-sectional field emission scanning electron microscopy (FESEM) samples were prepared by cleaving nanoPPX films that were immersed in liquid nitrogen for 30 min. High-resolution images were obtained to characterize the nanostructured morphology of Ni and Co films using a JEOL 6700F FESEM operating at a 3 kV acceleration voltage.

2.5.3. FIB. The Ni thickness measurement was performed using a focused ion beam (FEI Quanta 200 3D, OR) of Ga^+ impinging on the metal surface with 30 kV of kinetic energy. To minimize the surface damage, a thick layer of Au was sputtered onto the Ni layer before attempting FIB. After the removal of Ni from the surface, the film was imaged using an in situ scanning electron microscope (SEM) to measure the thickness of the Ni film. All images were taken at a 30° sample tilt.

2.5.4. XPS. To characterize the surface chemistry of the film after every chemical-modification step, X-ray photoelectron spectroscopy (XPS) was performed using an Axis Ultra XPS system (Kratos) that uses a monochromatic Al Kα X-ray source at a 20 eV pass energy with a 700 μm × 300 μm hybrid sample spot size and a 90° takeoff angle. The sample chamber was maintained under ultrahigh vacuum (10^{-9} Torr, 1 Torr = 133.322 N m^{-2}). The C 1s peak at 284.6 eV was used as the reference by which to analyze all of the collected spectra. The CasaXPS (version 2.3.14) software supplied by the manufacturer was used to analyze the data. The Pd 3d region was deconvoluted after nonlinear (Shirley-type) background subtraction and using a Gaussian/Lorentzian = 85/15 fit. To determine the photoelectric peak positions and concentrations, the following constraints were used: ratio of areas of Pd $3d_{5/2}$/Pd $3d_{3/2}$ = 1.5; binding-energy difference = Pd $3d_{3/2}$ − Pd $3d_{5/2}$ = 5.25 eV; the fwhm of all deconvoluted peaks within each spin−orbit coupling doublet was held constant.

2.5.5. XRD. The XRD data was obtained using a Scintag X2 X-ray diffractometer with a Cu Kα radiation source and a Si(Li) Peltier-cooled detector. The diffraction patterns were taken using grazing angle incidence (2° angle of incidence) while the detector was scanned from 5 to 45° at a rate of 0.02 deg s^{-1}.

2.5.6. QCM. Quartz crystal microbalance (QCM) measurements were carried out using a 5 MHz crystal with gold electrodes (QCM-100, SRS Inc., CA), an impedance analyzer (Agilent 4294A), and a QCM crystal holder (Maxtec Inc., NY). A layer of an octadecanethiol (C18-thiol) self-assembled monolayer (SAM)[46] was deposited on the gold electrode before depositing the PPX film onto it. The impedance magnitude and phase angle were recorded using a Labview data acquisition program, and the calculation to find the frequencies was made in a Mathematica 5.2 program.

Pyridine adsorption isotherms were measured for planar and nanoPPX films using vapor-phase adsorption at 298 K. A QCM crystal coated with nanoPPX or a planar film was horizontally suspended above an aqueous pyridine solution in a sealed vial. The entire assembly was kept in a vibration/acoustic-free isolation chamber. The vial was incrementally dosed with pyridine to increase the concentration stepwise from 0 to 1.5 M. The corresponding stabilized frequency, $f_{stab} \equiv (df/dt)_{f_{stab}} \leq 3$ Hz h^{-1}, at each step was recorded to plot the adsorption isotherm. The adsorption isotherms were normalized with respect to the corresponding thicknesses t of the planar (8.41 μm) and nanoPPX (7.12 μm) films.

2.5.7. Catalytic Activity. The catalytic activity of the Co-coated helical nanoPPX films was evaluated by measuring the volume of hydrogen released from the catalytic decomposition of alkaline-stabilized $NaBH_4$ solution as mentioned in our previous work.[13] Briefly, a 1 wt % NaOH (aq) solution (0.261 M) was prepared, followed by the addition of an equal volume of 2.5 wt % $NaBH_4$ (0.677 M). The Co-coated helical nanoPPX film was then lowered into the resulting solution. The hydrogen that evolved was collected in an inverted water column, and the volume was recorded with respect to time at room temperature and pressure (RTP).

3. Results and Discussion

3.1. Metallization of Noncovalently Functionalized Nano-PPX. Oblique angle polymerization (OAP) involves the growth of polymer films using obliquely directed monomeric radicals on a substrate (Figure 1A). Structure evolution leading to the aligned nanorod morphology of a nanostructured poly(chloro-*p*-xylylene) (nanoPPX) grown by OAP is detailed elsewhere.[40] Briefly, during the initial stage of deposition, a thin layer of PPX is formed as a result of the high surface diffusion of the radicals on the substrate. Although this thin layer of PPX is devoid of any structure, it shows surface instabilities that act as nucleation sites for the growth of the polymer columns. These nucleation sites grow in an aligned manner as the polymerization progresses. This alignment of the polymer columns is due to the self-shadowing effect created by the obliquely directed monomer vapor. The final morphology consists of obliquely aligned PPX nanorods on the substrate with a density of approximately ~10^7 nanorods mm^{-2} (Figure 1B).[41] The nanostructured morphology can be tuned by controlling the deposition parameters and/or the functional groups on PPX. In contrast, conventionally deposited planar PPX films (i.e., without the directed flux) do not possess such morphology.

Adhering the PPX films to the Si substrate requires a modification of the silicon surface using an allyltrimethoxysilane

(45) Markowitz, M.; Baral, S.; Brandow, S.; Singh, A. *Thin Solid Films* **1993**, *224*, 242–247.

(46) Ishida, T.; Hara, M.; Kojima, I.; Tsuneda, S.; Nishida, N.; Sasabe, H.; Knoll, W. *Langmuir* **1998**, *14*, 2092–2096.

Scheme 1. Surface Effects Model of the Metallization of Poly(chloro-*p*-xylylene) (PPX) Films[a]

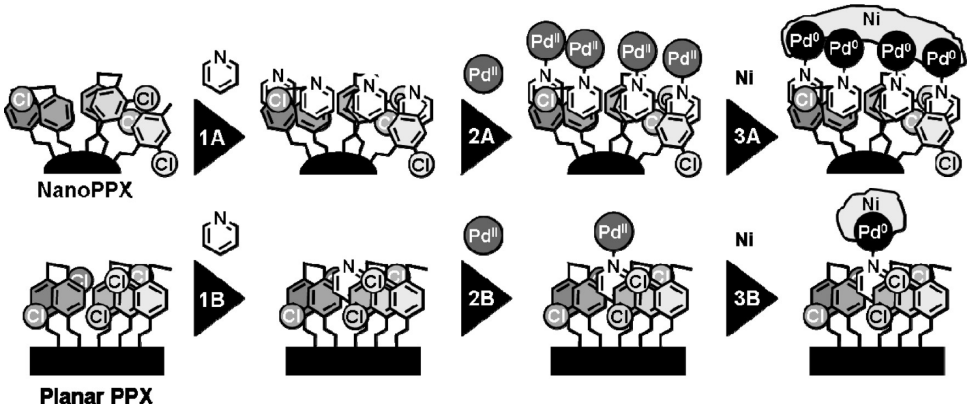

[a] Path A: nanostructured PPX films (nanoPPX). Path B: a planar PPX film.

self-assembled monolayer (SAM) as an adhesion promoter. The allyl group ($H_2C{=}CH{-}CH_2{-}$) chemically binds with the PPX film. One can directly deposit PPX films onto the Si substrate without using the SAM. However, because of the absence of any covalent bonding to the substrate and the hydrophobic nature of the polymer, the PPX films can easily delaminate in solvents such as water and ethanol. Because our work involves treating the films with aqueous solutions, it is necessary to establish good bonding between PPX and the silicon substrate, which is achieved through the covalent binding of the PPX to the SAM.

Figure 1C shows our three-step process for the electroless deposition of the Ni film on nanoPPX.[39] The electroless deposition of metal onto polymer surfaces usually requires prior treatment of the surface with a catalyst, which is often a colloidal Pd species.[5] One such species, PD1,[44] is a Pd(II)-based colloid formed by the controlled hydrolysis of $PdCl_4^{2-}$ species in aqueous solution. As the first step in our process, we physisorb a π-acceptor ligand, such as pyridine, onto the surface of the nanoPPX polymer. Subsequently, PD1 binds covalently and selectively to the N site of the pyridine molecule in both the Pd(II) state (via σ bonding) and the catalytically active Pd(0) state (via π back-bonding interactions) formed by reduction in an electroless plating bath.[5,47−49] Covalent binding of the catalyst increases the adhesion strength of the deposited electroless metal and improves the selectivity of the deposition compared to the use of conventional Pd/Sn catalysts.[5]

For pyridine impregnation of the nanoPPX film, we adopted two methods: the direct vapor method and partitioning from aqueous solution. In the first method, nanoPPX films are held in a chamber containing pyridine vapor, which adsorbs into the outermost layers of the nanostructured polymer film. In the second method, nanoPPX films are soaked into the aqueous pyridine solution to allow partitioning of the solvated pyridine molecules in the aqueous solution into the polymer. Because of the noncovalent nature of the adsorption interaction, the chemistry and favorable physicochemical properties of the nanoPPX polymer remain unaltered.

Scheme 1 illustrates our previously described model for pyridine physisorption, catalysis, and electroless metallization of nanoPPX films and planar PPX films.[39] In this model, the incorporation of pyridine in nanoPPX per path A, driven by

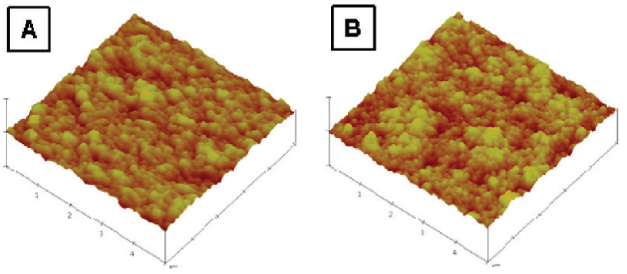

Figure 2. (A) Contact-mode AFM image of a pristine nanoPPX film. (B) Contact-mode AFM image of a Ni film deposited on nanoPPX functionalized using an aqueous pyridine treatment. Metallization parameters used for preparing sample B: (i) pyridine treatment condition, aqueous solution; (ii) pyridine adsorption time, 48 h; (iii) PD1 treatment time, 45 min; and (iv) Ni plating time, 60 min. For both AFM images, the unit length on the $x-y$ scale is 1 μm and the z-scale unit is 800 nm.

the minimization of the free energy for stabilization, occurs via the formation of favorable $\pi-\pi$ interactions with disordered aromatic groups comprising the polymer backbone at the largely amorphous surface regions of the PPX nanorods. Although $\pi-\pi$ interactions are weak, an array of multiple interactions, combined with covalent binding of the Pd catalyst, can create significant interface strength. As a result, metallized nanoPPX films using the noncovalent route consistently pass the Scotch tape adhesion test. Besides multiple noncovalent interactions, mechanical anchoring of the metal layer, as as result of the penetration of Ni into the spaces between the PPX nanorods, also contributes to the interface strength.[39] The AFM images in Figure 2 indicate that the metallization of the nanoPPX film occurs in a conformal manner, resulting in a metal layer that mimics the topology of the underlying polymer film. An SEM image (Figure 3) of the Ni film after Ga^+ focused ion beam (FIB) impingement shows a continuous Ni layer with thickness well under 100 nm (approximately 30−40 nm in thickness). Control samples of nanoPPX without ligands and/or PD1 treatment did not show any metallization, confirming that both ligand and PD1 treatments are necessary for metallization to occur. Although nanoPPX films exhibit excellent metallization with good interface strength, the conventionally deposited planar PPX films show no or poor metallization in a noncontinuous or patchy nature per Scheme 1, path B.[13,39] The poor metallization has been attributed to lower levels of pyridine adsorption in conventionally deposited planar PPX films, which lack the high-curvature surfaces that provide the disordered surface aromatic groups that facilitate pyridine incorporation into the nanoPPX films. Consequently, the lower concentration of pyridine

(47) Brandow, S. L.; Schull, T. L.; Martin, B. D.; Guerin, D. C.; Dressick, W. J. *Chem.—Eur. J.* **2002**, *8*, 5363–5367.
(48) Dressick, W. J.; Dulcey, C. S.; Georger, J. H.; Calabrese, G. S.; Calvert, J. M. *J. Electrochem. Soc.* **1994**, *141*, 210–220.
(49) Ada, E. T.; Hanley, L.; Etchin, S.; Melngailis, J.; Dressick, W. J.; Chen, M.-S.; Calvert, J. M. *J. Vac. Sci. Technol., B* **1995**, *13*, 2189–2196.

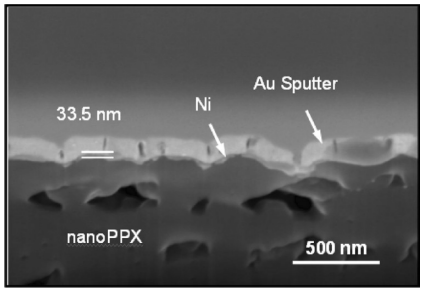

Figure 3. SEM image showing the cross-section of the Ni/nanoPPX composite film etched using FIB. Metallization parameters used to prepare samples: (i) pyridine treatment condition, aqueous solution; (ii) pyridine adsorption time, 48 h; (iii) PD1 treatment time, 45 min; and (iv) Ni plating time, 5 min.

molecules in planar PPX films simply cannot bind enough PD1 colloids to catalyze the Ni metallization.[39]

Unfortunately, the low pyridine levels in the PPX film preclude any direct evidence of the existence of $\pi-\pi$ interactions in the system through spectroscopic analysis.[50] Therefore, our assignment of $\pi-\pi$ interactions as the basis for the favorable binding of a ligand by nanoPPX films is rationalized by the chemical nature of the participating species and experimental observation. We eliminate electrostatic and hydrogen bonding as possible modes of interaction because the PPX structure does not contain functional groups that could support such interactions with the pyridine ligand. Conventional van der Waals interactions, though certainly present, are too weak in our system to support the strong binding evidenced by the adhesion tests that we observe. Specifically, we tested aliphatic ligands such as amylamine, which are capable of adsorption via conventional van der Waals interactions but not $\pi-\pi$ interactions. NanoPPX films treated with amylamine did show metallization indicative of adsorption on the nanoPPX surface but could not pass the Scotch tape adhesion test (Supporting Information, Figure S-1). In comparison, nanoPPX films treated with aromatic ligands such as pyridine and 4,4′-diphenyl-2,2′-dipyridyl consistently metallize the nanoPPX surface and exhibit excellent interface strength manifested by the Scotch tape adhesion test. It is also worth mentioning that ligand adsorption studies conducted using the QCM show that the frequency change for pyridine adsorption is 2 orders of magnitude higher than that for amylamine adsorption (Supporting Information, Figure S-2). Because frequency change scales directly to the mass of absorbent,[51] the quantity of pyridine molecules entering the PPX film is 2 orders of magnitude greater than the quantity of amylamine molecules. This again suggests that the $\pi-\pi$ interaction between an aromatic ligand such as pyridine and the aromatic backbone of the PPX polymer is the primary mode of the noncovalent interaction that binds the ligand molecules.

X-ray diffraction (XRD) results further support our mechanism for pyridine incorporation into these polymer films. PPX at room temperature exhibits a monoclinic α phase with a = 596 pm, b = 1269 pm, c (chain axis) = 666 pm, and β = 135.2.[40] Because the distance between two adjacent aromatic groups of the monoclinic PPX chain is 4.17 Å[52] and the stacking distance between the pyridine and benzene group is 3.7 Å,[53,54] it is unlikely that a pyridine molecule forms $\pi-\pi$ stacking interactions in the crystalline regime. Although both planar PPX and nanoPPX films possess crystalline regions, XRD experiments (Supporting Information, Figure S-3) signify the largely amorphous nature of the nanoPPX film. The large surface area and the high curvature of the PPX nanorods in a nanoPPX film result in polymer chains that are highly disordered at the surface. Specifically, the disordered polymer chains at the surface provide a mechanism to increase the accessibility of pyridine molecules into the nanoPPX polymer, consistent with the model in Scheme 1.

In contrast, the XRD pattern of a planar PPX film (Supporting Information, Figure S-3) shows a distinct peak at 2θ = 13.95° that is indicative of a (020) reflection from the monoclinic α phase. The XRD pattern of a planar PPX film indicates higher crystallinity compared to that of a nanoPPX film and preferential orientation of the monoclinic crystallites with the b axis perpendicular to the surface of the substrate. A planar PPX film has a lower surface area and a more compact and regular arrangement of the polymer chains compared to the chains in a nanoPPX film. Consequently, the pyridine adsorption rate in a planar PPX film is much lower than the rate of adsorption in a nanoPPX film, as illustrated by QCM adsorption kinetic curves (Supporting Information, Figure S-4). As a result, unlike the nanoPPX film, a planar PPX film at a typical pyridine adsorption time of ∼40−48 h exhibits poor or no metallization.[13,39] It should be noted that planar films kept in pyridine solution for much longer times (∼a week) also showed complete metallization. Such behavior is consistent with the slower trapping of pyridine ligands by the expected conformationally fluxional polymer chains at the PPX surface, resulting in the eventual accumulation of sufficient pyridine at the surface to bind PD1 in quantities necessary to promote electroless Ni deposition. A more detailed study of the crystallinity differences between the planar and nanoPPX film and its relation to the pyridine adsorption rate will be reported in a future publication.

The vapor-phase pyridine adsorption isotherms (Supporting Information, Figure S-5) obtained at 298 K on planar and nanoPPX films provide the equilibrium concentration of pyridine in the two films. The initial segment (0 mM < [pyridine] < 250 mM) of the adsorption isotherm of a nanoPPX film shows a nearly linear increase in pyridine concentration because of the adsorption of pyridine on the nanoPPX surface. Similar behavior is also observed for the planar PPX film, although the equilibrium concentration of pyridine in the planar PPX film is much lower. At [pyridine] ≈ 250 mM, a steep increase in pyridine adsorption is observed in the nanoPPX film and can be attributed to the capillary condensation of pyridine within the pores created by adjacent PPX nanorods.[55] In contrast, no such a behavior is observed for the planar PPX film because of the absence of such pores for pyridine condensation. The final segment ([pyridine] > 1 M) of the adsorption isotherm on the nanoPPX film is nearly linear as a result of the buildup of pyridine molecules on the outermost surface of the film culminating in adsorption saturation. The two adsorption isotherms indicate that the equilibrium concentration of pyridine is significantly higher (∼22 times at [pyridine] = 1 M) in nanoPPX than in the planar PPX film at any concentration. Such a drastic difference in the adsorption concentration translates into the observed difference in the metallization behavior of the two films.

3.2. Chemical Analysis. XPS analyses of the various chemical interactions in our system provide further evidence supporting

(50) Yang, D. Q.; Rochette, J. F.; Sacher, E. *J. Phys. Chem. B* **2005**, *109*, 4481–4484.
(51) Sauerbrey, G. *Z. Angew. Phys.* **1959**, *155*, 206–222.
(52) Senkevich, J. J.; Desu, S. B. *Polymer* **1999**, *40*, 5751–5759.
(53) Gao, S.; Huo, L.-H.; Shu, H.; Ng, S. W. *Acta Crystallogr., Sect. E* **2005**, *61*, m389–m391.
(54) Harrowfield, J. M.; Lugan, N.; Shahverdizadeh, G. H.; Soudi, A. A.; Thuery, P. *Eur. J. Inorg. Chem.* **2006**, 389–396.
(55) Qiao, S. Z.; Bhatia, S. K.; Zhao, X. S. *Microporous Mesoporous Mater.* **2003**, *65*, 287–298.

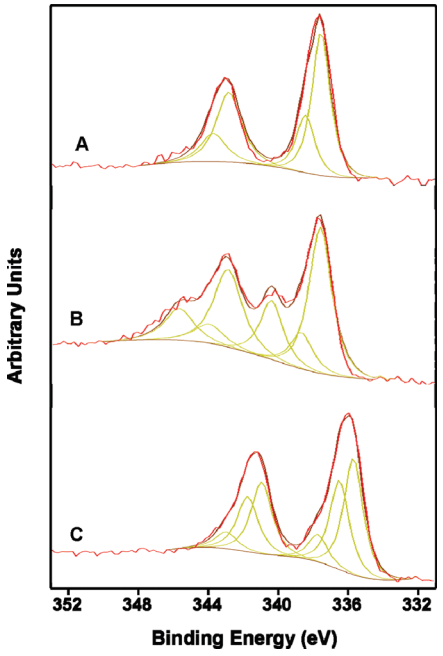

Figure 4. High-resolution XPS spectra of the Pd 3d region of (A) nanoPPX films treated with PD1 colloid for 30 min, (B) nanoPPX films treated with a 0.2 M aqueous pyridine solution for 30 min and PD1 for 30 min, and (C) the sample from part B after 5 min of treatment with NIPOSIT 468B.

our model. Figure 4 shows the Pd 3d region of PD1-treated nanoPPX films under three different conditions. We used the Pd $3d_{5/2}$ signal to assign the chemical states of Pd in the sample in each case. First, we treated nanoPPX films with PD1 catalyst for 30 min without any pretreatment with pyridine ligand solution and then rinsed the films in H_2O and dried them under N_2 gas before examining them with XPS. After background subtraction, the Pd $3d_{5/2}$ region was deconvoluted to fit two peaks at binding energies of 337.5 and 338.4 eV (Figure 4A). Because there is no ligand present in the structure of the PPX film, Pd(II) sites on the PD1 catalyst cannot covalently bind to the surface in this case. However, traces of PD1 are adsorbed to the surface in amounts insufficient to catalyze homogeneous electroless plating, consistent with behavior previously observed for this catalyst.[56] Consequently, the PD1 deposited here retains its inherent chemical composition unperturbed by ligand binding. The peaks at 337.5 and 338.4 eV can be assigned to Pd−O and Pd−Cl of the oxo/hydroxo and chloro-bridged Pd sites[57] of PD1. Literature values for the binding energy of Pd in PdO[58] and $PdCl_2$[59] closely match the binding energies assigned to Pd−O and Pd−Cl species in this work.

When nanoPPX films are treated with a 0.2 M aqueous pyridine solution for 30 min prior to treatment with PD1 for 30 min, the deconvoluted Pd $3d_{5/2}$ spectrum (Figure 4B) shows a strong peak at 340.3 eV in addition to the two peaks at 337.5 and 338.4 eV. The peak at 340.3 eV is an indication of Pd−N(pyridyl) interaction similar to that observed in other studies.[39,48] When the sample from Figure 4B is treated with 10% NIPOSIT 468B for 5 min, the entire Pd 3d spectrum shifts by ~2 eV toward lower

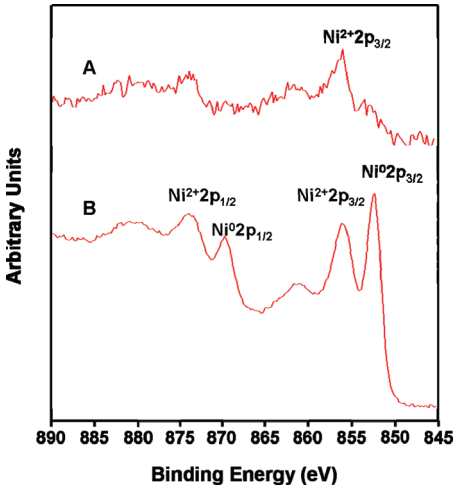

Figure 5. High-resolution XPS spectra of the Ni 2p region of (A) a nanoPPX film treated with a 0.2 M aqueous pyridine solution for 30 min, PD1 for 30 min, and NIPOSIT 468B for 5 min. (B) A nanoPPX film treated with 0.2 M aqueous pyridine solution for 40 h, PD1 for 30 min, and NIPOSIT 468B for 5 min.

binding energy (Figure 4C), indicating the reduction of divalent Pd by dimethylamine-borane (DMAB) present in the NIPOSIT electroless metallization bath. This reduced Pd state is a necessary condition for electroless metallization to occur.[57] However, the complexity of the signal, which requires three components to fit the band, indicates that other materials, such as PdO, unreduced Pd(II) species, and/or partially reduced Pd(I) species, in addition to metallic Pd(0), are likely present after reduction. Unfortunately, we are unable to unequivocally discern the nature of these species from our data.

Continuous Ni metallization requires a surface coverage of catalyst that exceeds a certain threshold limit, typically on the order of $\sim 10^{15}$ Pd(II) ions cm^{-2}.[48] To test the presence of the Ni layer on nanoPPX, a Ni 2p XPS spectrum was taken for three nanoPPX samples after plating. The first sample, which was not treated with pyridine, was treated directly with PD1 for 30 min and 10% NIPOSIT 468B for 5 min. The photoelectric spectrum did not show any peaks in the Ni 2p region (not shown), consistent with the lack of metallization visually observed. As explained previously, traces of PD1 (Pd = 0.39 atom %)[39] adsorbed by nanoPPX in the absence of ligand are not sufficient to surpass the above threshold and therefore cannot sustain metallization.

The second nanoPPX sample was treated with 0.2 M aqueous pyridine for 30 min prior to PD1 (30 min) and 10% NIPOSIT 468B (5 min) treatments. The XPS data shows only a weak peak (Ni = 0.28 atom %) at 856.3 eV (Figure 5A), indicating a thin, oxidized Ni layer. NanoPPX films treated with aqueous pyridine for a short time (30 min) can covalently bind PD1, as shown in the XPS data in Figure 4C. In this case, however, the amount of bound Pd is barely sufficient to initiate Ni deposition. Plating is readily quenched by dissolved oxygen and inhibitors in the electroless bath, leading to the deposition of thin, oxidized Ni films.

Results for a third sample, prepared using nanoPPX films treated with 0.2 M aqueous pyridine for 40 h, PD1 for 30 min, and 10% NIPOSIT 468B for 5 min, are shown in Figure 5B. The XPS spectrum shows a distinct Ni $2p_{3/2}$ peak (Ni = 5.90 atom %) at 852.3 eV (Figure 5B) indicating the presence of metallic Ni on the nanoPPX surface. In this case, a pyridine treatment time of ~40 h clearly leads to the subsequent binding of sufficient PD1 (Pd = 2.47 atom %) to support continuous Ni metallization.[39] The Ni

(56) Chen, M.-S.; Brandow, S. L.; Dulcey, C. S.; Dressick, W. J.; Taylor, G. N.; Bohland, J. F.; Georger, J. H.; Pavelchek, E. K.; Calvert, J. M. *J. Electrochem. Soc.* **1999**, *146*, 1421–1430.
(57) Charbonnier, M.; Romand, A.; Goepfert, Y.; Leonard, D.; Bessueille, F.; Bouadi, A. *Thin Solid Films* **2006**, *515*, 1623–1633.
(58) Militello, M. C.; Simko, S. J. *Surf. Sci. Spectra* **1994**, *3*, 395–401.
(59) Militello, M. C.; Simko, S. J. *Surf. Sci. Spectra* **1994**, *3*, 402–409.

$2p_{3/2}$ peak position observed is in excellent agreement with values previously reported for Ni metal in the literature.[60−64] The Ni $2p_{3/2}$ peak at 856.1 eV indicates the presence of a divalent Ni layer formed as a result of reaction with oxygen after exposure of the metallized sample to air. Several studies report similar peak positions for oxidized Ni, including those by Li (856.3 eV),[65] Zafeiratos (856.3 eV),[66] Sygellou (856.1 eV),[64] and Chow (856.1 eV),[62] consistent with our assignment.

3.3. Model Refinement. In an attempt to understand the degree of influence of the three metallization steps (shown in Figure 1C) on the morphology of the Ni film, we performed a 2^4 factorial analysis using the rms roughness as the quantitative measure of the Ni film morphology. Specifically, we studied four variables potentially affecting Ni roughness: pyridine adsorption time, PD1 binding time, Ni plating time, and pyridine adsorption conditions (i.e., aqueous pyridine or pyridine vapor treatment). A summary of the range of values investigated for each variable, the experimental roughness data obtained, and the statistical calculations and analysis of the effects are presented in the Supporting Information. The results of the factorial analysis reveal that all of the variables and their interactions, with the exception of the PD1 treatment time × Ni plating time interaction and the PD1 treatment time × pyridine adsorption time × pyridine adsorption condition interaction, are significant at the 99% confidence level and influence the surface morphology of the Ni film within the ranges of the variable specified. Such behavior clearly suggests that the growth of Ni on nanoPPX is a complex serial process where the ligand adsorption time, PD1 catalyst treatment time, Ni plating time, and ligand adsorption conditions interdependently affect the measured roughness of the Ni films. Among the factors examined, the pyridine adsorption condition had the highest impact on the morphology of the Ni film and these samples were further characterized using AFM, FESEM, and the catalytic activity measurement as discussed below.

Figure 6A,B shows the contact-mode AFM images of a Ni film deposited on nanoPPX films functionalized by aqueous and vapor-phase pyridine, respectively. The AFM images clearly suggest that sample 6B has a greater amount of roughness than sample 6A. The corresponding FESEM images of the two samples (Figure 6C,D, respectively) provide further insight into the mechanism involved in the formation of their respective final morphologies. The magnified image (Figure 6C, inset) shows the presence of a smooth Ni nanoparticle decorating an individual PPX nanorod. However, the inset of Figure 6D shows multiple Ni nanoparticles providing a rougher surface deposited onto a single PPX nanorod. The difference in the two morphologies is translated into different AFM roughness values observed for the two adsorption conditions. The dependence of the morphology on the ligand adsorption condition suggests that the amount of ligand adsorbed and the ligand molecule orientation in the polymer are factors that need further consideration.

In our previous work, we developed the simple model, summarized in Scheme 1, relating ligand adsorption to noncovalent $\pi-\pi$ interactions established between the ligand and disordered aromatic polymer chains present at the highly curved surfaces of

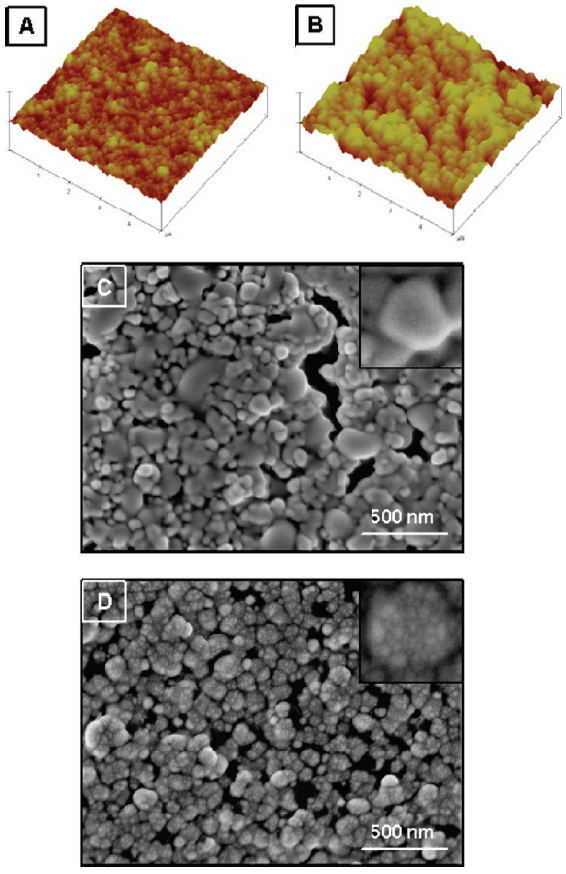

Figure 6. Contact-mode AFM image of a Ni layer deposited on nanoPPX films functionalized using (A) aqueous pyridine treatment and (B) vapor pyridine treatment. In each AFM image, the unit length on the $x-y$ scale is 1 μm and that on the z scale is 700 nm. FESEM image of Ni layers deposited on nanoPPX films functionalized using (C) the aqueous pyridine treatment and (D) the vapor pyridine treatment. (Insets in C and D) Magnified views of a single nanoPPX column with an inset square side of 100 nm. For the samples in all images, the ligand adsorption time is 30 h, the PD1 treatment time is 90 min, and the Ni plating time is 30 min.

the PPX nanorods.[39] We now further refine that simple model, using the observed FESEM and AFM results from Figure 6, to account for the differences in Ni film morphology observed for the vapor and aqueous pyridine treatment conditions. According to that model, partitioning of the pyridine molecules from the aqueous solution phase into the nanoPPX occurs without any external activation primarily because of the difference in the chemical potential of pyridine in the aqueous and bound states. Under these conditions, the degree of penetration and the amount of pyridine adsorbed will be limited because energy is required to break the hydrogen bonds solvating the hydrophilic N site of the pyridine molecule before it can fully enter the hydrophobic nanoPPX film. The presence of a hydrated N site is also expected to orient the ligand preferentially during insertion to keep the hydrophilic N ligand site in contact with the aqueous interface. The presence of this solvent shell may also provide a steric effect that limits the packing density of the ligand at the aqueous−PPX interface, countering the orientation effect. We observe the attachment of PD1 having a broad particle size distribution at high surface coverage in our work. Such behavior is consistent with the presence of ligand at high surface coverage,[67] suggesting

(60) Kukula, P.; Cerveny, L. *Appl. Catal., A* **2002**, *223*, 43–55.
(61) Shutthanandan, V.; Saleh, A. A.; Smith, R. J. *Surf. Sci.* **2000**, *450*, 204–226.
(62) Chow, Y. M.; Lau, W. M.; Karim, Z. S. *Surf. Interface Anal.* **2001**, *31*, 321–327.
(63) Sirtori, V.; Lombardi, L.; Cavallotti, P. L.; Magagnin, L. *Appl. Surf. Sci.* **2003**, *217*, 163–169.
(64) Sygellou, L.; Zafeiratos, S.; Tsud, N.; Matolin, V.; Kennou, S.; Ladas, S. *Surf. Interface Anal.* **2002**, *34*, 545–549.
(65) Li, L. B.; An, M. Z.; Wu, G. H. *Surf. Coat. Technol.* **2006**, *200*, 5102–5112.
(66) Zafeiratos, S.; Kennou, S. *Surf. Sci.* **2001**, *482*, 266–271.
(67) Brandow, S. L.; Dressick, W. J.; Marrian, C. R. K.; Chow, G. M.; Calvert, J. M. *J. Electrochem. Soc.* **1995**, *142*, 2233–2243.

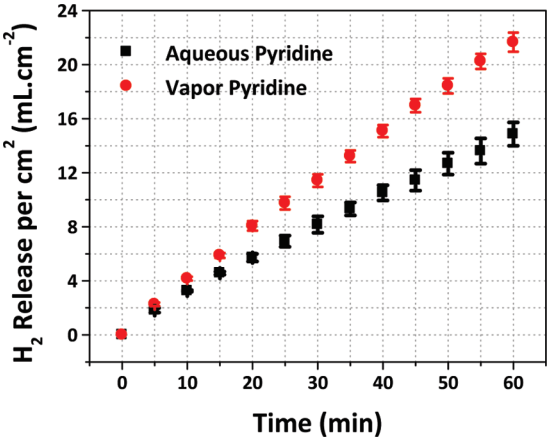

Figure 7. Hydrogen collected from the catalytic decomposition of alkaline-stabilized aqueous $NaBH_4$ solution using a Co film deposited on helical nanoPPX templates treated with aqueous and vapor-phase pyridine as catalysts. Metallization parameters: ligand adsorption time, 48 h; PD1 treatment time, 45 min; and Co plating time, 60 min. The hydrogen volume was measured at room temperature and pressure (RTP). Hydrogen volume raw data was normalized to the area of the catalyst film. Error bars represent one standard error of the mean.

that orientation rather than steric effects dominate in our system under aqueous conditions.

In contrast, the vapor deposition of pyridine is a thermally assisted process and therefore results in a greater adsorption of pyridine molecules in the nanoPPX film. However, because of the absence of any solvent, the molecules can penetrate the PPX film more deeply and take more random orientations than for aqueous ligand adsorption. Therefore, although larger quantities of pyridine may be incorporated via vapor deposition, fewer N-ligand sites may be accessible at the aqueous−PPX interface to bind PD1. The lower density of available N-ligand sites at the interface in this case is expected to lead to the binding of less PD1 catalyst overall and preferential binding of the smaller catalyst particles from the PD1 particle distribution, as observed previously in related systems.[67]

Consequently, different Ni film morphologies are expected and observed for samples treated with aqueous pyridine compared to those treated with vapor pyridine. During electroless plating, metal growth is initiated isotropically from the surface of each Pd(0) nanoparticle site on the surface. For the samples treated with aqueous pyridine, larger Pd(II) nanoparticles will be bound at higher surface coverage because of the relatively high surface density of accessible pyridine N sites present. As the Ni metal fronts proceed outward from each Pd site, it will quickly encounter metal fronts from adjacent Pd nanoparticles and merge. As a result, voids between Pd sites will quickly fill with Ni metal, leading to a relatively smooth Ni surface consistent with our observations in Figure 6A,C.

In contrast, the lower density of pyridine N sites accessible to the aqueous PD1 catalyst dispersion for the vapor-deposited ligand is expected to bind fewer and smaller Pd(II) nanoparticles. Consequently, Ni deposition will be slower and Ni metal fronts will require longer times to meet and merge because of the increased average distance between surface Pd sites. Given a fixed Ni plating time as described for Figure 6, fewer Ni fronts will have merged for the samples prepared by vapor pyridine deposition compared to the number prepared by aqueous pyridine deposition. Consequently, a rougher Ni surface is expected as observed in Figure 6B,D. It should be noted that for longer plating times

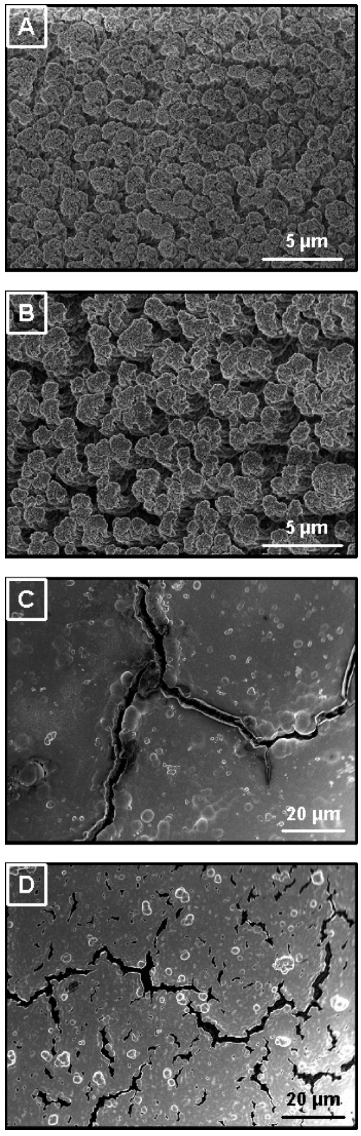

Figure 8. FESEM images showing the topography of a Co film deposited on helical nanoPPX films treated with (A) aqueous and (B) vapor-phase pyridine, respectively, after 1 min of Co plating. The scale bar for both images is 5 μm. FESEM images showing the topography of the Co film deposited on helical nanoPPX films treated with (C) aqueous and (D) vapor-phase pyridine, respectively, after 60 min of Co plating. The scale bar for both images is 20 μm.

the Ni surface on the vapor-pyridine-treated nanoPPX film will and does eventually become more smooth as the electroless metal fronts merge, consistent with the properties of the catalyst and the electroless Ni bath.

3.4. Catalytic Activity. Although we have demonstrated a nanoPPX template method for the formation of conformal metal films having controlled roughness using Ni metal, other metals such as Cu, Co, Fe, Au, Ag, Pt, and Pd and their alloys can be deposited onto the PPX nanorods after ligand adsorption and Pd(II) catalyst treatment. Next, we illustrate a practical application of controlled metal surface roughness by measuring the catalytic activity of electrolessly deposited Co films on nanoPPX templates. We have previously shown that Co films function as effective catalysts for hydrogen production from alkaline-stabilized $NaBH_4$ solution for hydrogen storage and fuel-cell applications.[13] Helical instead of columnar nanoPPX films were used to deposit Co to eliminate any effect due to the spatial

nonuniformity of the thickness in columnar nanoPPX films. Helical nanoPPX films can be prepared by introducing axial substrate rotation (i.e., $\omega > 0$; Figure 1C) in addition to the obliquely directed monomer vapor flux during film deposition.[43] Pyridine ligand (aqueous or vapor treatment) and PD1 treatment times were kept constant at 48 h and 45 min, respectively, for both samples. Co plating was carried out for short (1 min) and long (60 min) periods of time.

Figure 7 shows the hydrogen production obtained from a unit area of the Co films prepared from vapor and aqueous pyridine-treated helical nanoPPX substrates plated for 60 min. The hydrogen release shows an approximately linear increase in the volume of hydrogen as a function of time. By using a linear curve fit through the observed data points, the hydrogen release rate was calculated. Clearly, the Co film deposited on vapor-pyridine-treated nanoPPX films has a higher hydrogen release rate (0.37 mL min^{-1} cm^{-2}) than the Co film deposited on aqueous-pyridine-treated nanoPPX films (0.25 mL min^{-1} cm^{-2}). To understand in detail the reasons for the observed difference in the catalytic activity, we studied the topographical microstructures of the two films using FESEM. Figure 8A,B shows FESEM images of Co-coated (1 min in a Co plating bath) nanoPPX films treated with aqueous and vapor-phase pyridine, respectively. The FESEM images indicate that during Co deposition the topography of the underlying helical nanoPPX film is maintained. In other words, during initial stages of Co growth, Co nanoparticles cover the nanoPPX conformally. At longer bath times, however, the Co film grown on the vapor-treated nanoPPX film has a higher porosity because of the slower growth of the metal fronts (Figure 8D) compared to that of the Co film grown on the aqueous-pyridine-treated nanoPPX film that shows fused metal fronts (Figure 8C). This behavior is consistent with the refined model of Ni film growth described in section 3.3. The smaller nanoparticles and higher porosity of the Co film deposited on vapor-pyridine-treated nanoPPX film translate into higher catalytic activity because of the larger number of active reaction sites.[68]

4. Conclusions

We have employed noncovalent ligand functionalization on oblique-angle-polymerized nanoPPX templates to deposit metal nanoparticles and electroless metal films. Pyridine serves as the functional ligand, and a Pd(II) colloid that covalently binds to the pyridyl N sites seeds the metallization process in our nanoPPX system. Experimental evidence supports a model in which noncovalently bound pyridine molecules are stabilized via $\pi - \pi$ interactions with the disordered aromatic entities of the PPX chains in the amorphous surface domains of the nanoPPX film. The adsorption of pyridine into these sites is sufficient to support the complete conformal metallization of the surface. A refined model in which pyridine ligand orientation at the nanoPPX surface, controlled primarily by the pyridine adsorption condition (aqueous solution vs vapor phase), is described and accounts for the final morphology of the metal deposited. Other factors such as ligand adsorption time, PD1 treatment time, and metal plating time are also shown to influence the morphology of the metal layer, as suggested by a statistical investigation conducted using a 2^4 factorial analysis. Although a certain level of control over the metal morphology is possible by modifying the deposition parameters at the polymer preparation and/or the metal plating stages, challenges include expanding the generality of this method of functionalization to other polymer/ligand systems based on noncovalent interactions besides $\pi-\pi$ stacking.

The noncovalent functionalization of polymers prepared by OAP has several advantages over conventional covalent functionalization techniques, including the following: (1) noncovalent bonds are reversible and therefore have the ability to functionalize the surface reversibly without adversely affecting the material's desirable physicochemical properties; (2) a generic nanoPPX template is versatile and can create a family of porous materials, including metals[13] and ceramics,[69] using an appropriate ligand and/or deposition bath; and (3) because of the presence of high-energy surfaces in nanoPPX films, the ligand adsorption is readily controlled and temporally stable under ambient conditions.[39] Although the polymer/metal composite structure involves weak noncovalent interactions, the interface does not show any sign of adhesive weakness.[39] Such behavior is ascribed to the expected mechanical interlocking between the deposited metal and the polymer nanostructure as well as the larger number of noncovalent binding interactions as noted elsewhere for analogous noncovalent-based systems.[42]

PPX-templated composites, such as those described here, have promising applications in various emerging technologies. For example, Co membranes grown on the nanoPPX film show a highly interconnected porous structure that can be used as a catalyst for hydrogen production in fuel cells.[13] Ag or Au films deposited on nanoPPX films can be used as surface-enhanced Raman spectroscopy (SERS) substrates for biodetection with high signal sensitivity and reproducibility.[70,71] Bioceramics such as TiO_2 can also be deposited on nanoPPX films and have potential applications in orthopedic implant coatings.[69] The ability to control the nanostructured morphology and interfacial properties of the material layer coating the nanoPPX film is a prerequisite in all of these applications. We are continuing our efforts to understand better the properties of these hybrid systems to encourage the development of current and emerging applications.

Acknowledgment. This work was supported by the Pennsylvania State University and the Office of Naval Research under the Naval Research Laboratory Core 6.1 Research Program and the Young Investigator Program (MCD). We gratefully acknowledge Professor David L. Allara for allowing us access to the QCM equipment in his laboratory and Mr. Ping Kao for assisting in data collection.

Supporting Information Available: SEM image of a Ni film deposited on an amylamine-functionalized nanoPPX film. QCM frequency versus time data for amylamine and pyridine adsorption. XRD pattern of planar and nanoPPX films. Adsorption rate of pyridine in planar and nanoPPX films. Pyridine adsorption isotherm for planar and nanoPPX films. Detailed calculations of the factorial analysis. This material is available free of charge via the Internet at http://pubs.acs.org.

(68) Rhee, C. K.; Kim, B.-J.; Ham, C.; Kim, Y.-J.; Song, K.; Kwon, K. *Langmuir* **2009**, *25*, 7140–7147.

(69) Malvadkar, N.; Dressick, W. J.; Demirel, M. C. *J. Mater. Chem.* **2009**, *19*, 4796–4804.

(70) Kao, P.; Malvadkar, N. A.; Cetinkaya, M.; Wang, H.; Allara, D. L.; Demirel, M. C. *Adv. Mater.* **2008**, *20*, 3562–3565.

(71) Demirel, M. C.; Kao, P.; Malvadkar, N.; Wang, H.; Gong, X.; Poss, M.; Allara, D. L. *Biointerphases* **2009**, *4*, 35–41.